Received June 15, 2018, accepted July 22, 2018, date of publication July 31, 2018, date of current version August 20, 2018.

Digital Object Identifier 10.1109/ACCESS.2018.2860594

Wideband Patch Antenna Using Multiple Parasitic Patches and Its Array Application With Mutual Coupling Reduction

KAI DA XU[1,2,3], (Member, IEEE), JIANFENG ZHU[4], SHAOWEI LIAO[3,5], (Senior Member, IEEE), AND QUAN XUE[3,5], (Fellow, IEEE)

[1]Department of Electronic Science, Xiamen University, Xiamen 361005, China
[2]State Key Laboratory of Millimeter Waves, Southeast University, Nanjing 210096, China
[3]Shenzhen Key Laboratory of Millimeter-Wave and Wideband Wireless Communications, City University of Hong Kong, Shenzhen Research Institute, Shenzhen 518057, China
[4]State Key Laboratory of Millimeter Waves, Department of Electronic Engineering, City University of Hong Kong, Hong Kong
[5]School of Electronic and Information Engineering, South China University of Technology, Guangzhou 510641, China

Corresponding author: Quan Xue (eeqxue@cityu.edu.hk)

This work was supported in part by the National Natural Science Foundation of China under Grant 61601390, in part by the State Key Laboratory of Millimeter Waves Open Research Program under Grant K201813, in part by the Fundamental Research Program of Shenzhen City under Grant JCYJ20160608153614297, and in part by the Technology Research Project of Shenzhen City under Grant JSGG20150331154209122.

ABSTRACT A dual-layer patch antenna using multiple parasitic patches for the bandwidth enhancement is presented. Two additional resonances can be obtained with the help of the parasitic patches of the antenna. Consequently, a wide impedance bandwidth of 17% ($|S_{11}| < -10$ dB) can be achieved. Then, without the increase of the antenna array footprint, the combinations of two decoupling techniques (i.e., metalized via walls and short-circuited stepped-impedance structures as the neutralized networks) are adopted for mutual coupling reduction when the antenna element is extended to 2×1, 2×2, and even 4×4 array applications. To validate the design idea, a 2×2 antenna array is fabricated and tested, whose measured isolations between any two feeding ports are better than 28 dB within the frequency range of 3–4 GHz. The measured peak gain fluctuates from 12.6 to 13.6 dBi within the 10-dB impedance band of 3.35–3.95 GHz, and the cross-polarization levels in both the E- and H-planes are lower than -38 dB at the boresight direction.

INDEX TERMS Antenna array, decoupling technique, mutual coupling, parasitic patches, patch antenna, short-circuited stepped-impedance structure.

I. INTRODUCTION

Microstrip patch antenna has been researched and explored extensively in the past four decades due to its advantages of low profile, light weight, easy fabrication and conformability [1]–[3]. One of the most concerns for the patch antenna development focuses on the bandwidth enhancement [4]–[14] since it inherently suffers from narrow bandwidth limitation due to its single resonance radiation and high Q. Many approaches have been investigated to achieve wideband patch antennas for practical applications, of which two main ways can be summarized. One is inserting slots and/or pins to make the fundamental and harmonic resonances close to each other [4]–[8], while the other technique is adding parasitic strips/patches on the same layer or on the upper layer for the generation of new resonances [9]–[14].

When the patch antennas are employed for the array application, the problem of mutual couplings among antenna elements needs to be tackled since it will inevitably decrease the antenna efficiency and cause difficulties in achieving predefined radiation patterns. Various methods have been presented for the mutual coupling reduction in an array environment, of which two prevailing techniques can also be summarized as follows. One is that embedding a variety of different parasitic structures as the decoupling walls to suppress surface wave propagation between antenna elements. For instance, metal slabs and electromagnetic band gap (EBG) periodic structures are employed to diminish surface wave propagation in [15], [16], and [17], respectively, resulting in the reduction of mutual coupling between closely spaced radiating elements. In [18], a waveguide metamaterial

scheme is utilized to decouple two neighboring microstrip patches with 6-dB mutual coupling reduction. The other main method is introducing the decoupling networks between antenna elements to neutralize the intrinsically mutual coupling, resulting in the achievement of high isolations and good input return losses simultaneously. Many different kinds of decoupling neutralized networks have been proposed such as those using distributed- and lumped-element circuits [19], microstrip transmission lines [20], [21] and coupled resonators [22], [23].

In this paper, a wideband patch antenna on the two substrate layers and its array application are presented. Two additional resonances can be obtained with the help of four parasitic patches positioned on the top layer of the antenna, which enhances the bandwidth. For the area miniaturization of antenna, two parasitic patches along the radiating edge direction are short-circuited to the metalized via walls. In terms of dealing with the mutual coupling problem when extended to array application, we adopt the combinations of the two above mentioned techniques, i.e., decoupling walls and neutralized networks. The metalized via walls can not only make the above two parasitic patches short-circuited easily, but also suppress surface wave propagation as the decoupling walls to mitigate the detrimental mutual coupling among the antenna elements. Moreover, simple decoupling short-circuited stepped-impedance structures (SSISs) as the neutralized networks are added for further mutual coupling reduction.

The remained parts of this paper are organized as follows. In Section II, a dual-layer wide patch antenna with multiple parasitic patches and metalized via walls is designed and analyzed. Then, it can be easily employed for the design of antenna array, and hence a 2×2 array with simple SSISs for the mutual coupling reduction is explored and experimentally measured in Sections III. Finally, a brief conclusion is given in Section IV.

II. DUAL-LAYER PATCH ANTENNA DESIGN

As illustrated in Fig. 1, the proposed dual-layer patch antenna is designed using two substrate layers whose relative permittivity are both 2.65, and substrate thicknesses of h_1 and h_2 are 1.5 and 2 mm, respectively. The fed patch (denoted as *FP* in the figure) at the center of the first metal layer (M1) is fed by the coaxial probe, and four parasitic patches (i.e., *PP1*, *PP2*, *PP3* and *PP4*) are also positioned on M1. All structures of the antenna are within the square cavity formed by metalized vias as its side walls. Here, the two substrate layers are utilized to easily embed the decoupling SSISs in the array application, which will be seen in Section III. Full-wave electromagnetic simulations are implemented by Ansys HFSS [24]. The parameters of the antenna are tabulated in Table 1. The design procedure is described as follows.

First, a coaxial-fed single patch antenna is designed with only one resonance and the electrical length of its radiating edge (physical parameter *fy* in Fig. 1(a)) is smaller than $\lambda_g/2$ due to the relatively large substrate thickness and

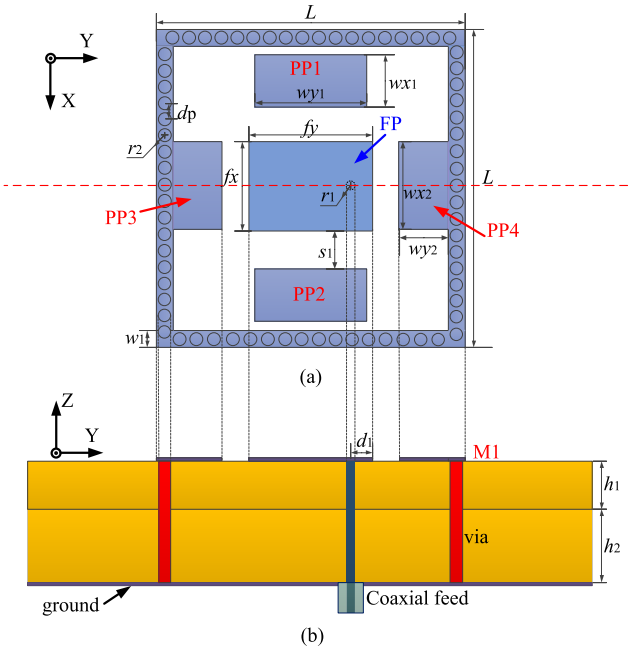

FIGURE 1. Geometry of the proposed dual-layer wideband patch antenna element. (a) Top view, and (b) cross sectional view along the dash red line in (a).

TABLE 1. Parameters of the dual-layer patch antenna in millimeters.

wx_1	9	wy_2	9.9	L	62	d_1	6.9	dp	2.7
wy_1	23.2	fx	19	w_1	2.8	r_1	0.65	h_1	1.5
wx_2	18.4	fy	25.2	s_1	8.7	r_2	1.2	h_2	2

fringing field effect, where λ_g is the guided wavelength in the dielectric medium at the resonance frequency. The resonance frequency f_{r1} introduced by fed patch *FP* is located at around 3.44 GHz as seen in Fig. 2(a).

Then, when two parasitic patches *PP1* and *PP2* along the non-radiating edges (x-direction) are added based on the single patch antenna with fed patch (*FP*), a second resonance at f_{r2} is introduced, thus two resonances at around f_{r1} and f_{r2} can be obtained as shown in Fig. 2(a). Furthermore, another two parasitic patches *PP3* and *PP4* along its radiating edges (y-direction) are added for generating a third resonance at f_{r3}. For size reduction, they are both short-circuited to the metalized via walls, whose length wy_2 can be decreased in half, from around half-wavelength to quarter-wavelength at the resonance of parasitic patch *PP3* (or *PP4*) due to electrical wall effect of the via walls. In addition to the short-circuited facilitation, the square cavity using metalized via walls also can mitigate the detrimental mutual coupling among the antenna elements when it is extended to the design of the antenna array, which will be introduced in Section III. Fig. 2(b) illustrates simulated input impedance curves on Smith chart, which agree well with the $|S_{11}|$ evolution of the proposed antenna in Fig. 2(a). To demonstrate the wide

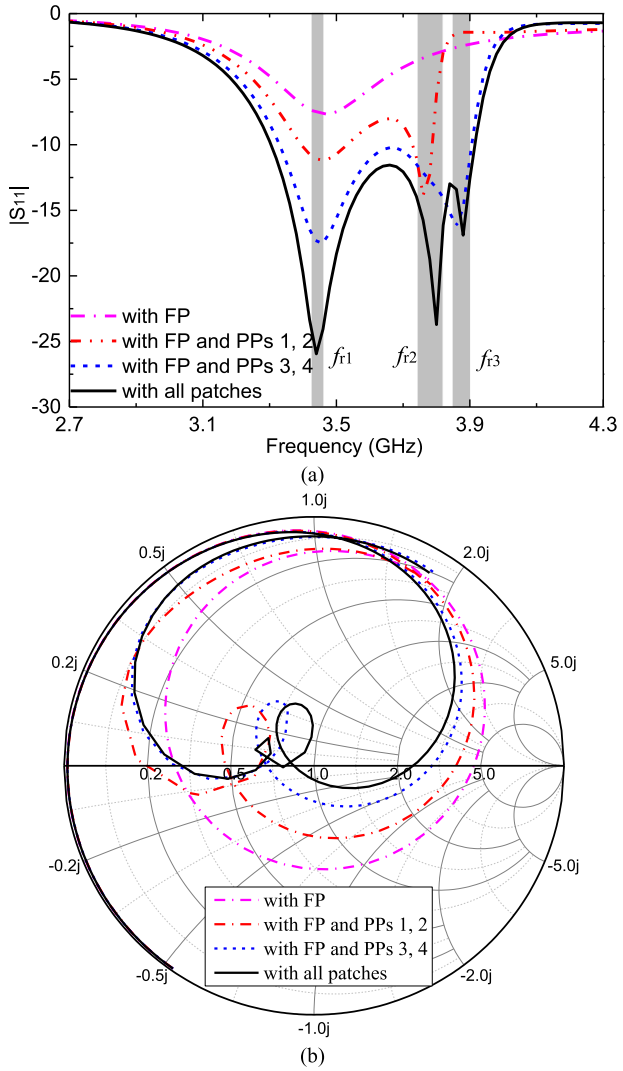

FIGURE 2. (a) Simulated $|S_{11}|$ frequency responses and (b) simulated input impedances on Smith chart of the four antennas with different numbers of PPs. The common parameters are identical.

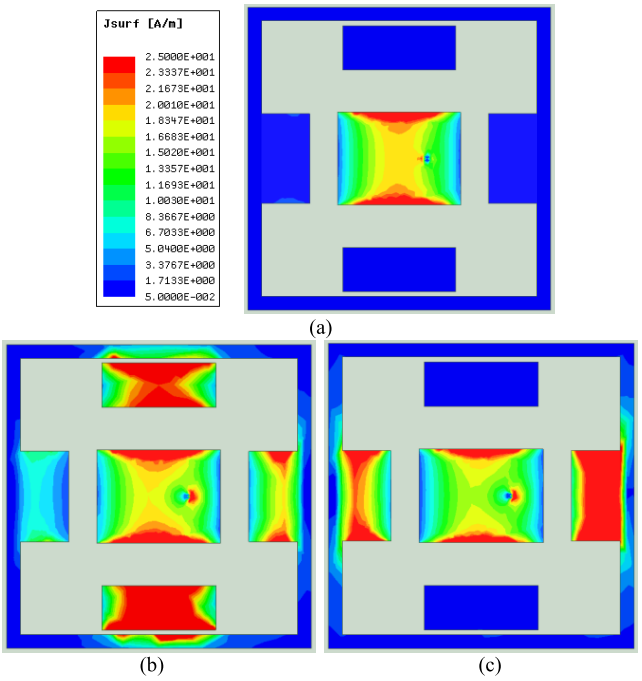

FIGURE 3. Simulated surface current distributions of the proposed antenna element at (a) $f_{r1} = 3.44$, (b) $f_{r2} = 3.8$, and (c) $f_{r3} = 3.88$ GHz.

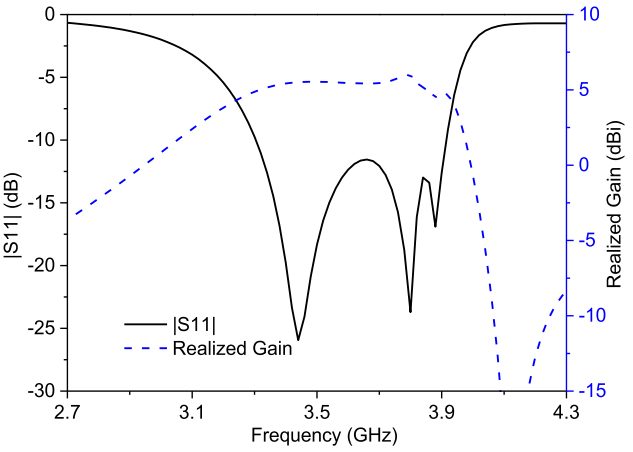

FIGURE 4. Simulated $|S_{11}|$ and realized gain at boresight direction of the antenna element.

impedance bandwidth, surface current distributions at three different frequencies (i.e., f_{r1}, f_{r2} and f_{r3}) are shown in Fig. 3. In Fig. 3(a), the fed patch *FP* contributes to the resonance f_{r1}, while in Fig. 3(b), the intense currents at f_{r2} are mainly located on the fed patch *FP* and two parasitic patches (*PP1* and *PP2*), where the energy could be coupled from the fed patch *FP* to the parasitic patches *PP1* and *PP2* to improve the impedance bandwidth and gain in upper band. At f_{r3}, the maximum currents distributing along the fed patch *FP*, parasitic patches *PP3* and *PP4* in Fig. 3(c), show that the parasitic patches *PP3* and *PP4* play an important role in the generation of the third resonancef_{r3}. Finally, three resonances at 3.44, 3.8, and 3.88 GHz are combined together to enlarge the impedance bandwidth.

From the above analysis, it is predicted that three resonances will be acquired if all the parasitic patches are positioned on the M1 layer to construct the proposed antenna as shown in Fig. 1. The simulated $|S_{11}|$ frequency response of the proposed antenna in Fig. 2(a) with three resonances f_{r1}, f_{r2} and f_{r3} validates the design idea. Note that the parameters $fx+2(s_1 + wx_1 + w_1) < L$ should be satisfied since the parasitic patches *PP1* and *PP2* are not connected to the metalized via walls. Fig. 4 illustrates the simulated reflection coefficient, and realized gain at boresight direction of the proposed patch antenna. A wide −10 dB impedance bandwidth of 17% from 3.3 to 3.91 GHz can be achieved with the center frequency at 3.605 GHz. The simulated radiation patterns in the E-plane (*yz*-plane) and H-plane (*xz*-plane) at three operating frequencies 3.3, 3.6, 3.9 GHz are shown in Fig. 5.

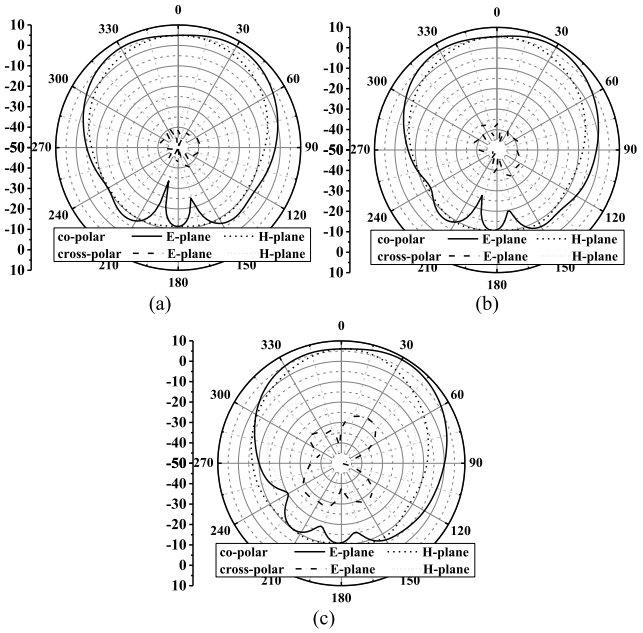

FIGURE 5. Simulated radiation patterns in the E- and H-planes at (a) 3.3 GHz, (b) 3.6 GHz, and (c) 3.9 GHz.

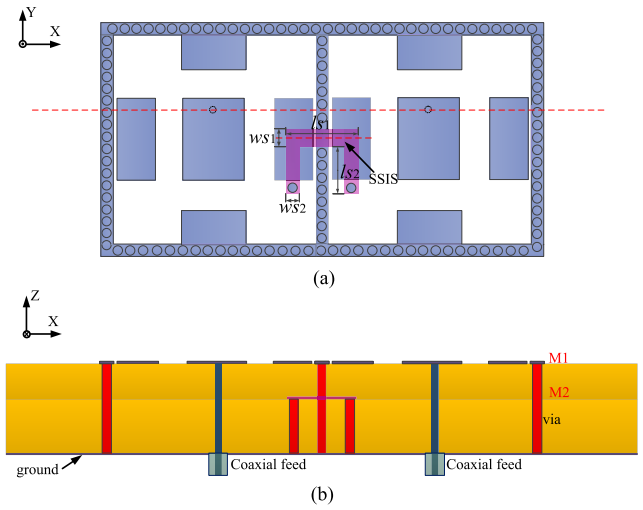

FIGURE 6. Geometry of the horizontal 2 × 1 antenna array with decoupling structure. (a) Top view, and (b) cross sectional view along the long dash red line in (a). SSIS in the geometry denotes short-circuited stepped-impedance structure.

III. ARRAY APPLICATION

A. HORIZONTAL 2 × 1 ANTENNA ARRAY

When the proposed dual-layer wideband patch antenna is employed in the 2 × 1 antenna array, there are two ways of array placement, i.e., horizontal and vertical, which are electric coupling and magnetic coupling dominant conditions as seen in this subsection A and next subsection B, respectively. Fig. 6 shows the horizontal 2 × 1 antenna array towards x-direction with a simple SSIS for the mutual coupling reduction. The metalized via walls for surface wave propagation suppression can mitigate the detrimental mutual coupling between these two antenna elements, but the isolation is still not high enough. To further reduce mutual coupling, a simple symmetrical stepped-impedance structure as the neutralized network is positioned at the center of the second metal layer (M2) and short-circuited to the ground.

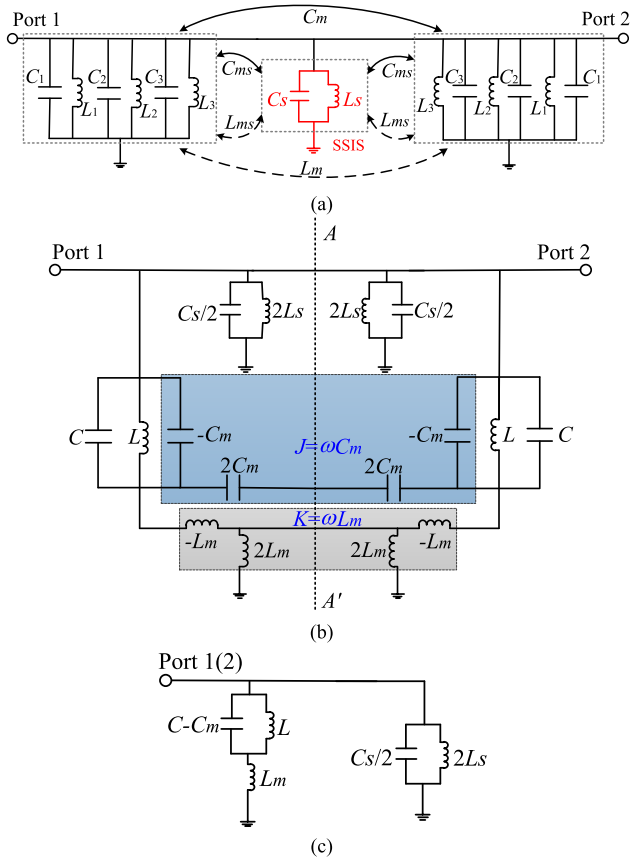

FIGURE 7. (a) Equivalent circuit model of the 2 × 1 antenna array with the SSIS. (b) Transformed equivalent circuit without taking into account of the electric and magnetic coupling between the antenna element and SSIS. (c) Simplified equivalent circuit of (b).

Fig. 7 illustrates the equivalent circuit model of the 2 × 1 antenna array with the SSIS, where all losses are not taken into account for simplicity. Each patch antenna element is represented by three parallel LC tanks (L_1C_1, L_2C_2 and L_3C_3) since it has three resonances, whereas the parallel L_sC_s tank represents the SSIS. The three parallel LC tanks (L_1C_1, L_2C_2 and L_3C_3) can be simplified by one parallel LC tank in which $C = C_1 + C_2 + C_3$ and $L = (1/L_1 + 1/L_2 + 1/L_3)^{-1}$. The electric and magnetic couplings between the two patch antenna elements (LC) are denoted by the mutual capacitance C_m and mutual inductance L_m, whereas the electric and magnetic couplings between the patch antenna element (LC) and SSIS (L_sC_s) are denoted by the mutual capacitance C_{ms} and mutual inductance L_{ms}, respectively. Since the values of the parametersC_{ms} and L_{ms} are very small compared with those of C_m and L_m, they can be ignored in the equivalent circuit. According to equivalent circuit theory [25], [26], a transformed equivalent circuit can be derived as shown in Fig. 7(b), where the mutual inductance L_m and mutual

capacitance C_m are represented by an impedance inverter $K = \omega L_m$ and an admittance inverter $J = \omega C_m$, respectively.

Due to the symmetry structure, the odd- and even-mode analysis method can be adopted to further simplify the transformed equivalent circuit [27]. By inserting an electric wall at the symmetrical A-A' plane, the odd-mode circuit is fully short-circuited and hence it does not exist. Therefore, the even-mode circuit will be the finally simplified equivalent circuit as seen in Fig. 7(c), whose input admittance is derived as

$$Y_{\text{in}} = [\frac{j\omega L}{1-\omega^2(C-C_m)L} + j\omega L_m]^{-1} + \frac{j\omega C_s}{2} + \frac{1}{2j\omega L_s}. \quad (1)$$

For the ideal 2 × 1 patch antenna array without any mutual coupling, the input admittance of either antenna element port (i.e., Port 1 or Port 2) can be expressed by

$$Y_{\text{ideal}} = j\omega C + \frac{1}{j\omega L}. \quad (2)$$

To obtain the perfect decoupling effect, the input admittance in (1) should be as close as possible to the one in (2), i.e., $Y_{\text{in}} \approx Y_{\text{ideal}}$. Actually, the introduction of the parameters L_s and C_s aims to neutralize the influence of the mutual inductance L_m and mutual capacitance C_m.

Finally, the parameters of the SSIS are optimized to set as $l_{s1} = 27.4$ mm, $l_{s2} = 15.2$ mm, $w_{s1} = 3.7$ mm, $w_{s2} = 7.9$ mm, and the diameters of the short-circuited vias are all 2 mm. Fig. 8 compares three cases of S-parameters versus frequencies, where −10 dB impedance bandwidths of these three cases are basically the same, all from 3.3 to 3.9 GHz. When the metalized via walls are inserted between two antenna elements as Case II, $|S_{11}|$ can reach up to −20 dB within the passband except the frequency range of 3.8-3.86 GHz as seen in Fig. 8. For the isolation, more than 5 dB reduction of mutual coupling at 3.3-3.55 GHz can be achieved comparing with that of Case I. Furthermore, based on Case II, the SSIS is coupled to the input and output ports as the neutralized network instead of direct connection to the input and output ports [20], thus the design of antenna structure is more flexible. Over 4 dB reduction of mutual coupling at the frequency range of 3.3-3.89 GHz and even 11.5 dB improvement at 3.87 GHz will be acquired. Consequently, more than 26 dB isolation can be achieved within the passband of 3.3-3.9 GHz.

B. VERTICAL 2 × 1 ANTENNA ARRAY

Similarly, a vertical 2 × 1 antenna array towards y-direction with another short-circuited stepped-impedance structure (i.e., SSIS' in Fig 8(a)) for the mutual coupling reduction is also designed. As shown in Fig. 9, the parameters of this structure are set as $l'_{s1} = 15$ mm, $l'_{s2} = 9.4$ mm, $w'_{s1} = 4$ mm, $w'_{s2} = 5.4$ mm, and the diameters of the short-circuited vias are also 2 mm.

Fig. 10 compares another three cases of S-parameters versus frequencies for the vertical 2 × 1 antenna array.

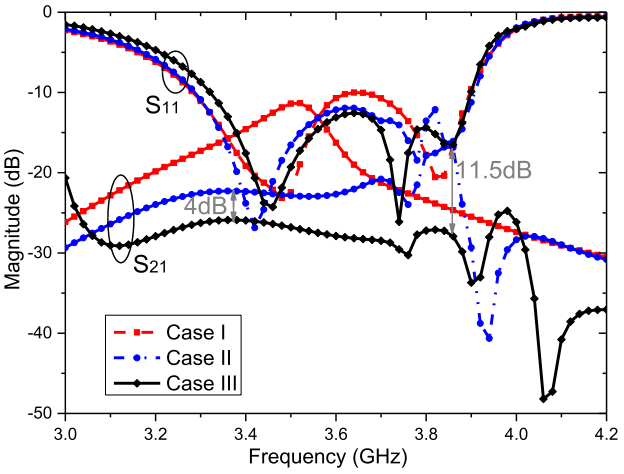

FIGURE 8. Simulated isolations between two antenna elements and reflection coefficients of three antenna array cases. Case I: horizontal 2 × 1 antenna array without any decoupling structure; Case II: horizontal 2 × 1 antenna array with via walls; Case III: horizontal 2 × 1 antenna array with via walls and the SSIS.

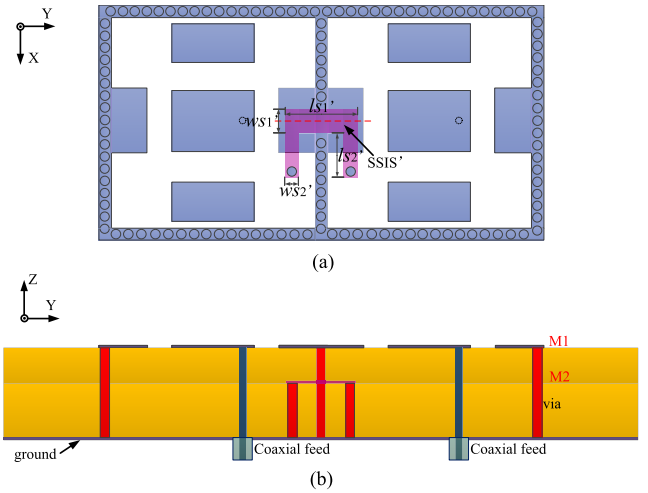

FIGURE 9. Geometry of the vertical 2 × 1 antenna array with decoupling structure. (a) Top view and (b) cross sectional view. SSIS' in the geometry denotes another short-circuited stepped-impedance structure.

The -10 dB impedance bandwidths of these three cases almost keep the same, around from 3.3 to 3.88 GHz. For Case B with the metalized via walls, the isolation can be significantly improved in the frequency range of 3.3-3.8 GHz compared with that of Case A. When the SSIS is embedded on the M2 layer as Case C, 2 dB more reduction of mutual coupling within the whole band, and even 19 dB improvement at 3.85 GHz can be obtained. Consequently, the isolation of over 20.5 dB between two elements of this antenna array can be achieved within the whole passband.

C. 2 × 2 ANTENNA ARRAY

Combining the above two 2 × 1 antenna arrays, as shown in Fig. 11, a 2 × 2 antenna array can be easily achieved with mutual coupling reduction among all the antenna elements

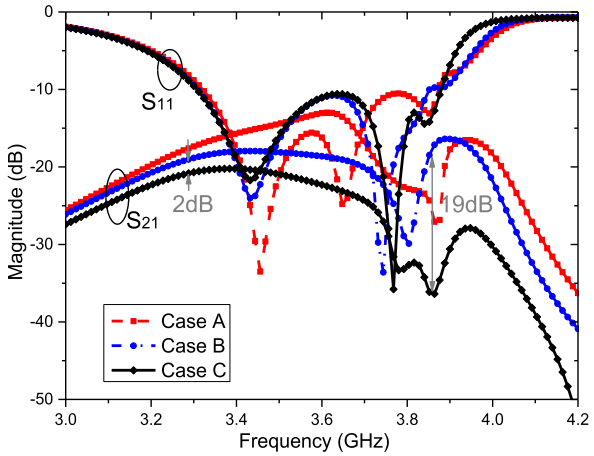

FIGURE 10. Simulated isolations between two antenna elements and reflection coefficients of three antenna array cases. Case A: vertical 2 × 1 antenna array without any decoupling structure; Case B: vertical 2 × 1 antenna array with via walls; Case C: vertical 2 × 1 antenna array with via walls and the SSIS.

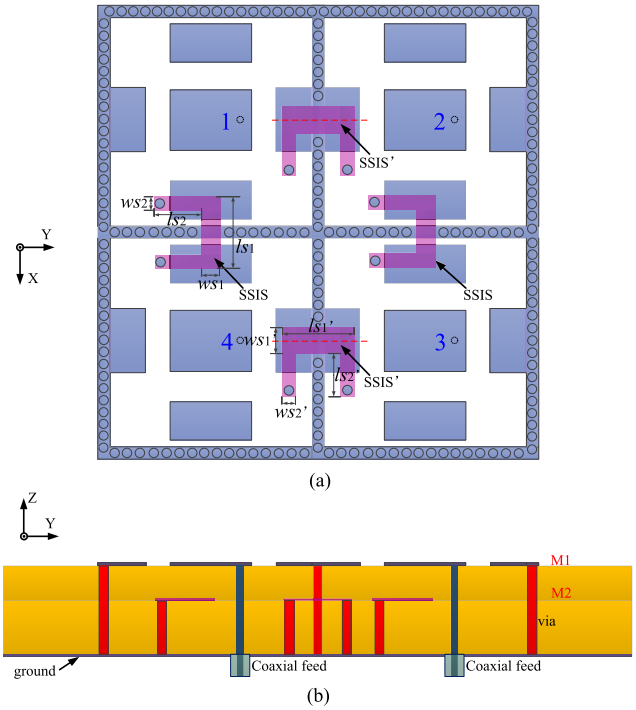

FIGURE 11. Geometry of the 2 × 2 antenna array with decoupling structure. (a) Top view and (b) cross sectional view.

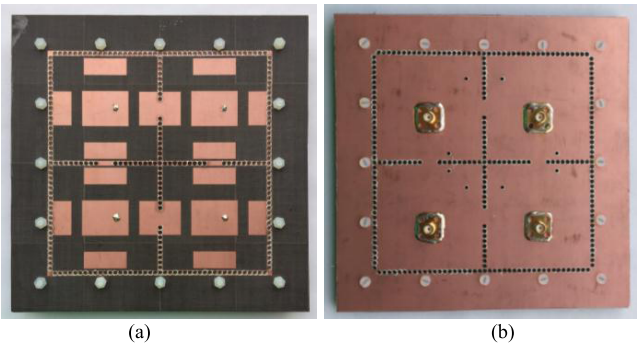

FIGURE 12. Photograph of the fabricated 2 × 2 array. (a) Top view, and (b) bottom view.

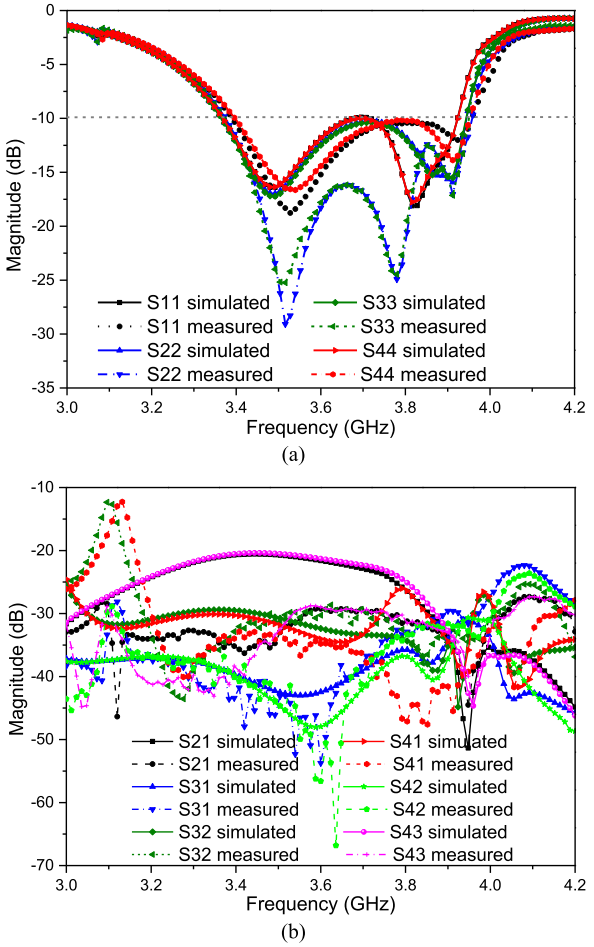

FIGURE 13. S-parameters of the 2 × 2 antenna array with decoupling structure. (a) Reflection coefficients and (b) isolations.

using decoupling walls and neutralized networks simultaneously, where all the parameters do not need to be re-tailored. It is fabricated through printed circuit board (PCB) process, whose fabricated photograph is shown in Fig. 12. Two substrate boards are stacked and fixed together by plastic screws. The overall size of the proposed array is 160 mm × 160 mm × 3.5 mm.

The simulated and measured reflection coefficients at all ports of the 2 × 2 antenna array are illustrated in Fig. 13(a). It shows that the simulated impedance matchings of better than −10 dB are from 3.36 to 3.93 GHz for all four ports, and the measured counterparts are from 3.38 to 3.95 GHz. The slight discrepancy between simulations and measurements may be attributed to the manufacturing tolerance and probe soldering of coaxial-fed connector.

Fig. 13(b) plots the simulated and measured isolations among all the antenna elements. The simulated isolations between any two ports are over 20 dB at the frequency

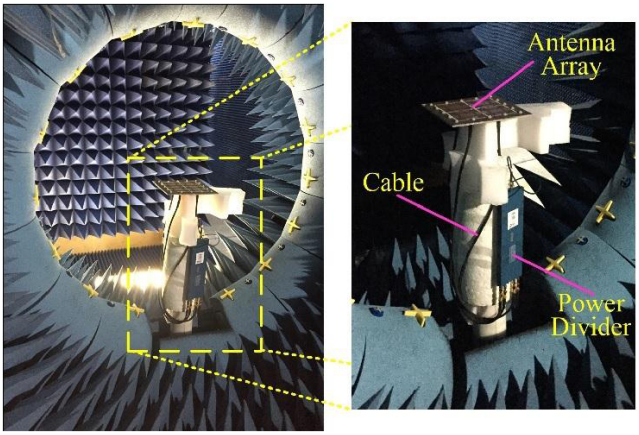

FIGURE 14. Measurement setup of radiation patterns in the SATIMO StarLab.

range from 3 to 4.2 GHz. In contrast, the measured isolations between any two ports are even better than 28 dB at the frequency range of 3-4 GHz. The differences are mainly caused by the fabricated errors, assembling deviations of dual-layer substrate and tolerance of via walls during metalized process. For the isolations of antenna array, it is reasonable that the performance of measured results surpasses the simulations.

D. FAR-FIELD EXPERIMENTAL RESULTS

In order to measure far-field radiation characteristics of this 2 × 2 antenna array whose four input ports are fed with the same magnitude and in-phase, a four-way equal power divider with bandwidth of 0.5-26.5 GHz from Krytar Inc. [28] is employed whose four output ports are connected to the four input ports of the fabricated 2 × 2 antenna array. The radiation pattern of the antenna array has been measured by SATIMO StarLab system, the setup of which is shown in Fig. 14.

The simulated and measured radiation patterns in the E-plane and H-plane at the frequency points of 3.4, 3.65, and 3.9 GHz are shown in Fig. 15, which are all normalized to the peak gains. It can be seen that the measured results are mostly in good agreement with the simulations. The measured cross-polarization levels in both E- and H-planes are lower than −38 dB at the boresight direction. Fig. 16 plots the comparisons of simulated and measured peak gains of the proposed antenna arrays with different scales, i.e., 1 × 1, 2 × 1 and 2 × 2. The measured peak gain of 2 × 2 antenna array fluctuates from 12.6 to 13.6 dBi within the 10-dB impedance band of 3.35-3.95 GHz.

Performance comparisons are conducted between our work and some recently reported patch antennas as tabulated in Table II. It can be seen that our presented study has realized wide impedance bandwidths, high peak gains, low cross polarizations and high front-to-back ratios simultaneously.

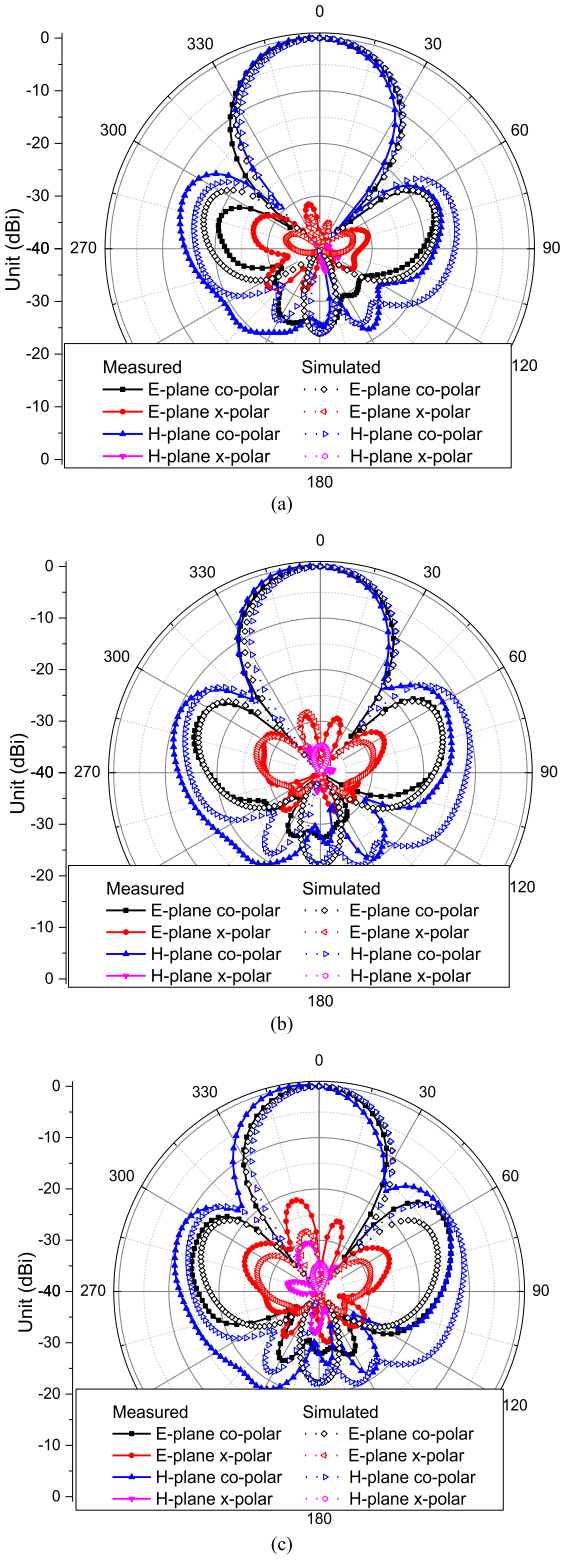

FIGURE 15. Simulated and measured radiation patterns (normalized) of the 2 × 2 array in the E- and H-planes at (a) 3.4 GHz, (b) 3.65 GHz, and (c) 3.9 GHz.

E. DISCUSSIONS

Furthermore, the proposed antenna can be easily extended to the design of large-scale antenna arrays (e.g., 4 × 4, 16 × 16 arrays), whose feeding networks can be designed separately and positioned beneath the ground of the antenna. Fig. 17 shows the radiation patterns of antenna element,

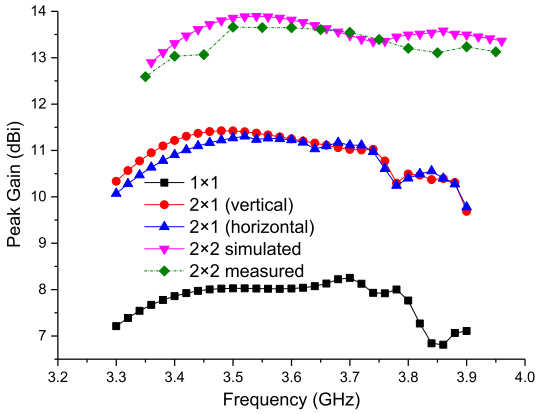

FIGURE 16. Comparisons of simulated and measured peak gains among these four proposed antenna arrays.

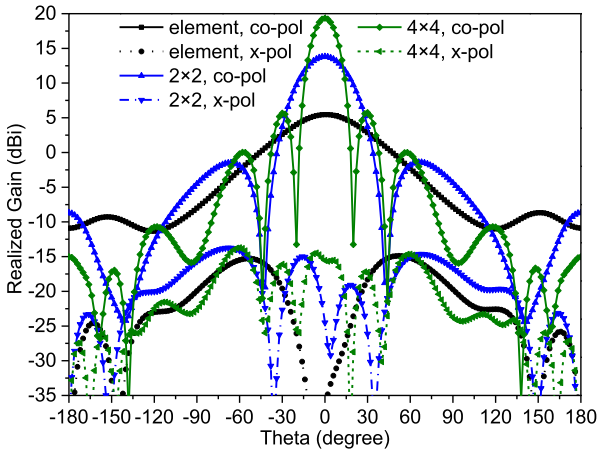

FIGURE 17. Simulated radiation pattern comparisons of antenna element, 2 × 2 array and 4 × 4 array at 3.6 GHz.

TABLE 2. Comparisons with some previous patch antennas.

	-10 dB bandwidth	Front-to-back ratio	Cross polarization	Peak gain	Size (λ_0^3)
[8]	11.8%	~9 dB	-21 dB	3 dBi	0.82×0.48×0.042
[10]	12.3%	~18 dB	NM*	2 dBi	0.14×0.14×0.06
[12]	17.4%	12 dB	NM	3 dBi	0.72×0.78×0.03
[14]	19.5%	NM	-22 dB	9.8 dBi	0.92×0.92×0.03
This work (antenna element)	**17%**	**14.6 dB**	**-43 dB**	**8 dBi**	**0.74×0.74×0.04**
This work (measured 2×2 array)	**16%**	**25 dB**	**-38 dB**	**13.6 dBi**	**1.42×1.42×0.04**

*NM: Not Mentioned.

2 × 2 array and 4 × 4 array at 3.6 GHz in H-plane with all feeding ports in phase. It illustrates that these three antennas have the maximum radiation at the boresight direction, and their realized gains are 5.7, 13.8, and 19.4 dBi, respectively. The design of this antenna element aims to have

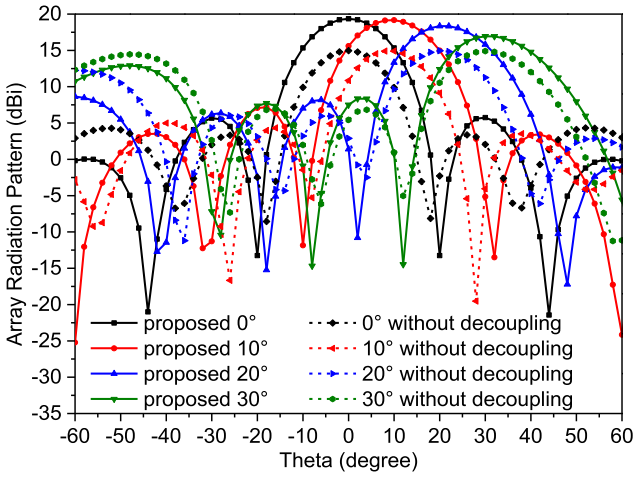

FIGURE 18. 4 × 4 array H-plane radiation patterns scanned to 0°, 10°, 20° and 30°.

broad beamwidth, resulting in the maximum realized gain of E-plane not at the boresight direction as seen in Fig. 5. Therefore, it is reasonable that the realized gain 5.7 dBi of antenna element at the boresight direction of H-plane is slightly smaller than the peak gain of 8 dBi shown in Fig. 16.

With broad beamwidth (64°) of the proposed antenna element, it can also be extended to the design of beam-scanning phased array. Fig. 18 illustrates the simulated 4 × 4 array radiation patterns in H-plane scanned to 0° (boresight direction), 10° , 20° and 30°, as well as its compared counterpart without decoupling structures. Obviously, the realized gain at the scanned angle will be deteriorated when the decoupling structures are not employed, about 5 dB gain loss at the boresight direction. Moreover, the grating lobe will be also reduced with the help of decoupling structures.

IV. CONCLUSION

A wideband patch antenna using multiple parasitic patches with three resonances is proposed, whose 10 dB impedance bandwidth is 17% from 3.3 to 3.91 GHz. Then, when the antenna is extended to array applications, a new decoupling technique with the combination of metalized via walls and the neutralized networks is explored, which does not increase the extra size of the antenna array. High measured isolations of over 28 dB between any two feeding ports validate the design idea. Owing to the simple design procedure, the proposed antenna and its arrays are attractive for use in the scanning phased arrays.

REFERENCES

[1] K.-L. Wong, *Compact and Broadband Microstrip Antennas*. New York, NY, USA: Wiley, 2002.
[2] G. Kumar and K. P. Ray, *Broadband Microstrip Antennas*. Norwood, MA, USA: Artech House, 2003.
[3] K. F. Lee and K. M. Luk, *Microstrip Patch Antennas*. London, U.K.: Imperial College Press, 2011.
[4] R. Chair, C. L. Mak, K.-F. Lee, K.-M. Luk, and A. A. Kishk, "Miniature wide-band half U-slot and half E-shaped patch antennas," *IEEE Trans. Antennas Propag.*, vol. 53, no. 8, pp. 2645–2652, Aug. 2005.

[5] A. Khidre, K. F. Lee, A. Z. Elsherbeni, and F. Yang, "Wide band dual-beam U-slot microstrip antenna," *IEEE Trans. Antennas Propag.*, vol. 61, no. 3, pp. 1415–1418, Mar. 2013.

[6] J. Liu, Q. Xue, H. Wong, H. W. Lai, and Y. Long, "Design and analysis of a low-profile and broadband microstrip monopolar patch antenna," *IEEE Trans. Antennas Propag.*, vol. 61, no. 1, pp. 11–18, Jan. 2013.

[7] J.-D. Zhang, L. Zhu, Q.-S. Wu, N.-W. Liu, and W. Wu, "A compact microstrip-fed patch antenna with enhanced bandwidth and harmonic suppression," *IEEE Trans. Antennas Propag.*, vol. 64, no. 12, pp. 5030–5037, Dec. 2016.

[8] N.-W. Liu, L. Zhu, W.-W. Choi, and X. Zhang, "Wideband shorted patch antenna under radiation of dual-resonant modes," *IEEE Trans. Antennas Propag.*, vol. 65, no. 6, pp. 2789–2796, Jun. 2017.

[9] W. S. T. Rowe and R. B. Waterhouse, "Investigation into the performance of proximity coupled stacked patches," *IEEE Trans. Antennas Propag.*, vol. 54, no. 6, pp. 1693–1698, Jun. 2006.

[10] C. Sun, H. Zheng, L. Zhang, and Y. Liu, "Analysis and design of a novel coupled shorting strip for compact patch antenna with bandwidth enhancement," *IEEE Antennas Wireless Propag. Lett.*, vol. 13, pp. 1477–1481, 2014.

[11] Z. Liang, J. Liu, Y. Zhang, and Y. Long, "A novel microstrip quasi Yagi array antenna with annular sector directors," *IEEE Trans. Antennas Propag.*, vol. 63, no. 10, pp. 4524–4529, Oct. 2015.

[12] K. D. Xu, H. Xu, Y. Liu, J. Li, and Q. H. Liu, "Microstrip patch antennas with multiple parasitic patches and shorting vias for bandwidth enhancement," *IEEE Access*, vol. 6, pp. 11624–11633, 2018.

[13] K. Ding, C. Gao, B. Zhang, Y. Wu, and D. Qu, "A compact printed unidirectional broadband antenna with parasitic patch," *IEEE Antennas Wireless Propag. Lett.*, vol. 16, pp. 2341–2344, 2017.

[14] K. Ding, C. Gao, D. Qu, and Q. Yin, "Compact broadband circularly polarized antenna with parasitic patches," *IEEE Trans. Antennas Propag.*, vol. 65, no. 9, pp. 4854–4857, Sep. 2017.

[15] B. A. Arand, A. Bazrkar, and A. Zahedi, "Design of a phased array in triangular grid with an efficient matching network and reduced mutual coupling for wide-angle scanning," *IEEE Trans. Antennas Propag.*, vol. 65, no. 6, pp. 2983–2991, Jun. 2017.

[16] F. Yang and Y. Rahmat-Samii, "Microstrip antennas integrated with electromagnetic band-gap (EBG) structures: A low mutual coupling design for array applications," *IEEE Trans. Antennas Propag.*, vol. 51, no. 10, pp. 2936–2946, Oct. 2003.

[17] H. S. Farahani, M. Veysi, M. Kamyab, and A. Tadjalli, "Mutual coupling reduction in patch antenna arrays using a UC-EBG superstrate," *IEEE Antennas Wireless Propag. Lett.*, vol. 9, pp. 57–59, 2010.

[18] X. M. Yang, X. G. Liu, X. Y. Zhou, and T. J. Cui, "Reduction of mutual coupling between closely packed patch antennas using waveguided metamaterials," *IEEE Antennas Wireless Propag. Lett.*, vol. 11, pp. 389–391, 2012.

[19] S. C. Chen, Y. S. Wang, and S. J. Chung, "A decoupling technique for increasing the port isolation between two strongly coupled antennas," *IEEE Trans. Antennas Propag.*, vol. 56, no. 12, pp. 3650–3658, Dec. 2008.

[20] C.-H. Wu, G.-T. Zhou, Y.-L. Wu, and T.-G. Ma, "Stub-loaded reactive decoupling network for two-element array using even–odd analysis," *IEEE Antennas Wireless Propag. Lett.*, vol. 12, pp. 452–455, 2013.

[21] Y.-F. Cheng and K.-K. M. Cheng, "A novel and simple decoupling method for a three-element antenna array," *IEEE Antennas Wireless Propag. Lett.*, vol. 16, pp. 1072–1075, 2017.

[22] L. Zhao, L. K. Yeung, and K.-L. Wu, "A coupled resonator decoupling network for two-element compact antenna arrays in mobile terminals," *IEEE Trans. Antennas Propag.*, vol. 62, no. 5, pp. 2767–2776, May 2014.

[23] L. Zhao and K.-L. Wu, "A dual-band coupled resonator decoupling network for two coupled antennas," *IEEE Trans. Antennas Propag.*, vol. 63, no. 7, pp. 2843–2850, Jul. 2015.

[24] *Ansys High Frequency Structural Simulator (HFSS) Version 16*, Ansys Corp., Framingham, MA, USA, 2016.

[25] J.-S. Hong and M. J. Lancaster, "Couplings of microstrip square open-loop resonators for cross-coupled planar microwave filters," *IEEE Trans. Microw. Theory Techn.*, vol. 44, no. 11, pp. 2099–2109, Nov. 1996.

[26] Q.-X. Chu and H. Wang, "A compact open-loop filter with mixed electric and magnetic coupling," *IEEE Trans. Microw. Theory Techn.*, vol. 56, no. 2, pp. 431–439, Feb. 2008.

[27] D. M. Pozar, *Microwave Engineering*, 2nd ed. New York, NY, USA: Wiley, 1998.

[28] *KRYTAR MLDD 4-Way Power Dividers*. [Online]. Available: https://krytar.com/

KAI DA XU (S'13–M'15) received the B.S. and Ph.D. degrees in electromagnetic field and microwave technology from the University of Electronic Science and Technology of China, Chengdu, China, in 2009 and 2015, respectively.

From 2012 to 2014, he was a Visiting Researcher with the Department of Electrical and Computer Engineering, Duke University, Durham, NC, USA, under the financial support from the China Scholarship Council. From 2016 to 2017, he was a Post-Doctoral Fellow with the State Key Laboratory of Millimeter Waves, City University of Hong Kong, Hong Kong. He is currently an Assistant Professor with the Institute of Electromagnetics and Acoustics, and the Department of Electronic Science, Xiamen University, Xiamen, China. He has authored and co-authored over 90 papers in peer-reviewed journals and conference proceedings. His current research interests include RF/microwave and mm-wave circuits, antenna arrays, and nanoscale memristors.

Dr. Xu was a recipient of the UESTC Outstanding Graduate Awards in 2009 and 2015, respectively. He was also a recipient of the National Graduate Student Scholarship in 2012, 2013, and 2014, from the Ministry of Education, China. Since 2017, he has been served as an Associate Editor for both of the IEEE Access and *Electronics Letters*. He is also an Editorial Board Member of the *AEÜ-International Journal of Electronics and Communications*. He is serving as a Reviewer for several IEEE and IET journals, including the IEEE Transactions on Microwave Theory and Techniques, the IEEE Transactions on Antennas and Propagation, the IEEE Transactions on Electron Devices, the IEEE Transactions on Computer-Aided Design of Integrated Circuits and Systems, the IEEE Antennas and Wireless Propagation Letters, the IEEE Microwave and Wireless Components Letters, the *IEEE Microwave Magazine*, the IEEE Access, *IET Microwaves Antennas and Propagation*, and *Electronics Letters*.

JIANFENG ZHU was born in Changsha, Hunan, China. He received the B.Eng. degree in communication engineering from the Beijing University of Posts and Telecommunications, Beijing, China, in 2013, where he is currently pursuing the Ph.D. degree. Since 2015, he has been a Research Assistant with the Department of Electronic Engineering, City University of Hong Kong. His research interests include mm-wave antennas and MIMO antennas.

SHAOWEI LIAO (M'13–SM'16) received the Ph.D. degree in electromagnetic fields and microwave technology from the University of Electronic Science and Technology of China (UESTC), Chengdu, China, in 2010. From 2007 to 2009, he was a Research Assistant with the Department of Electronics, Carleton University, Canada. In 2011, he was with the School of Electronic Engineering, UESTC, as a Lecturer. From 2011 to 2012, he served as a Senior Research Associate with the Department of Electronic Engineering, City University of Hong Kong, Hong Kong. From 2012 to 2013, he was at Bell Labs Research, China, Shanghai Bell, Alcatel-Lucent, as a Research Scientist. From 2013 to 2017, he was an Engineer with the State Key Laboratory of Millimeter Waves, City University of Hong Kong. In 2017, he joined the South China University of Technology, where he is currently an Associate Professor.

He has authored or co-authored over 20 internationally referred papers in IEEE journals. He is a Co-Inventor of five granted U.S./European/international patents, in addition to six filed patents. His research includes various antennas, computational electromagnetics, microwave components, and metamaterials. He was a recipient of 2017 H. A. Wheeler Applications Prize Paper Award. He is the Reviewer of the IEEE Transactions on Antennas and Propagation, the IEEE Antennas and Wireless Propagation Letters, and the IEEE Microwave and Wireless Components Letters.

QUAN XUE (M'02–SM'04–F'11) received the B.S., M.S., and Ph.D. degrees in electronic engineering from the University of Electronic Science and Technology of China (UESTC), Chengdu, China, in 1988, 1991, and 1993, respectively. In 1993, he joined UESTC as a Lecturer. He became a Professor in 1997. From 1997 to 1998, he was a Research Associate and a Research Fellow with The Chinese University of Hong Kong. In 1999, he joined the City University of Hong Kong and was a Chair Professor of microwave engineering. He also served as the Associate Vice President at the Innovation Advancement and China Office from 2011 to 2015, the Director of the Information and Communication Technology Center, and the Deputy Director of the State Key Laboratory of Millimeter Waves, Hong Kong. In 2017, he joined the South China University of Technology, where he is currently a Professor and also serves as the Dean of the School of Electronic and Information Engineering.

He has authored or co-authored over 300 internationally referred journal papers and over 130 international conference papers. He was the Co-Inventor of five granted Chinese Patents and 15 granted U.S. Patents, in addition to 26 filed patents. His research interests include microwave/millimeter-wave/THz passive components, active components, antenna, microwave monolithic integrated circuits, and radio frequency integrated circuits. He served the IEEE as an AdCom Member of MTT-S from 2011 to 2013. He was a recipient of 2017 H. A. Wheeler Applications Prize Paper Award. He was an Associate Editor of the IEEE TRANSACTIONS ON MICROWAVE THEORY AND TECHNIQUES from 2010 to 2013, the Editor of the *International Journal of Antennas and Propagation* from 2010 to 2013, and an Associate Editor of the IEEE TRANSACTIONS ON INDUSTRIAL ELECTRONICS from 2010 to 2015. He has been an Associate Editor of the IEEE TRANSACTIONS ON ANTENNA AND PROPAGATIONS since 2016.